

Vibrational excitation of water by electron impact

M. A. Khakoo

Department of Physics, California State University, Fullerton, California 92834, USA

C. Winstead and V. McKoy

A. A. Noyes Laboratory of Chemical Physics, California Institute of Technology, Pasadena, California 91125, USA

(Received 25 March 2009; published 28 May 2009)

Experimental and calculated differential cross sections (DCSs) for electron-impact excitation of the (010) bending mode and unresolved (100) symmetric and (001) antisymmetric stretching modes of water are presented. Measurements are reported at incident energies of 1–100 eV and scattering angles of 10° – 130° and are normalized to the elastic-scattering DCSs for water determined earlier by our group. The calculated cross sections are obtained in the adiabatic approximation from fixed-nuclei, electronically elastic scattering calculations using the Schwinger multichannel method. The present results are compared to available experimental and theoretical data.

DOI: [10.1103/PhysRevA.79.052711](https://doi.org/10.1103/PhysRevA.79.052711)

PACS number(s): 34.80.Bm, 34.80.Gs

I. INTRODUCTION

There has been considerable interest in electron scattering from water at low incident energies. More broadly, there has been renewed interest in studies of the interaction of slow electrons with biological tissue due to the recent work of Sanche and co-workers [1–3] demonstrating that such electrons can induce single- and double-strand breaks in DNA. Water is of course fundamentally important to electron-molecule collisions in biological environments because it is the primary constituent of living tissue, and energy loss to the vibrational modes of water is an important mechanism in the degradation of subexcitation electrons [4]. Electron-water collisions are also of practical interest in discharges, atmospheres, and interstellar and circumstellar media. In addition, water is a prototypical small polyatomic molecule whose large dipole moment makes it suitable for studies of dipole-related effects. Itikawa and Mason [5] critically reviewed experimental and theoretical data on the low-energy electron cross sections of water published prior to 2004.

Relative differential cross sections (DCSs) for electron-impact vibrational excitation of water at 15 eV and above were measured by Trajmar *et al.* [6]. Absolute DCSs for vibrational excitation were measured by Seng and Linder [7,8] at impact energies from threshold to 10 eV and scattering angles from 20° to 110° , and soon after by Rohr [9], who obtained excitation functions up to 3 eV and DCSs in the near-threshold region. Although not concerned with vibrational excitation, the early work of Jung *et al.* [10], who determined rotationally resolved, vibrationally elastic DCSs at 2.14 and 6.0 eV, should also be mentioned. Subsequent vibrational-excitation studies, not encompassing the near-threshold energy range, were carried out by Shyn *et al.* [11], Ben Arfa *et al.* [12], Furlan *et al.* [13], and El-Zein *et al.* [14,15]. Allan and Moreira [16] revisited the near-threshold region with an impressive energy resolution of 10 meV, sufficient to resolve the two stretching modes, (100) and (001) (with respective thresholds of 0.453 and 0.466 eV), measuring cross sections at a fixed scattering angle of 135° . At 1 eV, they found the symmetric stretch (100) cross section to be about five times larger than that of the asymmetric stretch

(001), while the rotational band profiles of the peaks in the energy-loss spectra at 0.6 eV residual energy suggested a resonant mechanism for excitation of the (100) mode (as well as for the bending mode) and a direct (dipolar) mechanism for excitation of the (001) mode. In contrast, Seng and Linder [7,8] and Rohr [9] deduced from the angular dependence of the DCSs a resonant mechanism for (100)+(001) excitation near threshold and a dipolar mechanism for (010) excitation. Recently, Makochekanwa *et al.* [17] obtained DCSs for vibrational excitation near 8 eV impact energy, where the scattering is influenced by a broad shape resonance. Although their energy resolution of 38 meV was insufficient to resolve the stretching modes, they deduced separate cross sections for the (100) and (001) modes by least-squares fitting of the unresolved energy-loss spectra to a sum of Gaussians representing the instrumental function.

Several calculations of the cross sections for vibrational excitation of water have been reported, beginning with that of Itikawa [18] in the first Born approximation. Jain and Thompson [19] computed (100) and (010) DCSs from 1 to 8 eV using the adiabatic approximation [20], with fixed-nuclei elastic cross sections obtained in a single-particle model that included local potentials to represent the exchange and polarization interactions between the projectile and target. Nishimura and Itikawa [21] employed a two-state vibrational close-coupling procedure, with the electronic degrees of freedom again treated in a single-particle picture relying on local exchange and polarization potentials. Moreira *et al.* [22] used the adiabatic approximation and treated the fixed-nuclei electronic problem via the *R*-matrix method, obtaining DCSs for excitation of the three vibrational modes below 10 eV. The same method was also employed by Allan and Moreira [16]. Čurík and Čárský [23] treated the two-state vibrational close-coupling problem via a discrete momentum representation in which the electronic problem is handled within the static-exchange approximation. Recently Nishimura and Gianturco [24] treated the vibrational close-coupling problem for water using a local model of the electronic potential and extending their calculations down to the near-threshold energy region. Makochekanwa *et al.* [17] carried out calculations using the adiabatic approximation and the continuum

multiple-scattering model in support of their cross-section measurements. In general, the calculated results for the bending mode (010) agree reasonably well with the measured cross sections, but agreement is less satisfactory for the (100)+(001) modes, particularly at low impact energies. Itikawa [25] reviewed computational work on vibrational excitation of water through 1997 and discussed the underlying theory.

In the present paper, we report measured DCSs for vibrational excitation of water over an extensive range of impact energies, namely, 1, 2, 4, 5, 6, 8, 10, 15, 20, 30, 50, and 100 eV, and at scattering angles from 10° to 130° . For comparison, we have also calculated the vibrational-excitation cross sections using the adiabatic approximation and treating the fixed-nuclei electronic problem via the Schwinger multi-channel (SMC) method [26,27] in the static-exchange plus polarization approximation. Our DCSs are used to compute integral cross sections (ICSs) and momentum-transfer cross sections (MTCs). We compare our results with available calculated and measured values.

II. METHOD

A. Experiment

The present experimental apparatus (spectrometer, vacuum chamber, and control equipment) has been described in detail in previous papers, e.g., by Khakoo *et al.* [28], and only a brief description will be given here. The electron gun and the detector employed double hemispherical energy selectors, and the apparatus was made of titanium. Cylindrical lenses were utilized, and the system was baked to about 130°C with magnetically free biaxial heaters (ARi Industries model BXX06B41-4K). The analyzer detector was a discrete dynode electron multiplier (Equipe Thermodynamique et Plasmas model AF151) with the extremely low background rate of <0.01 Hz and capable of linearly detecting >100 Hz without saturating. The remnant magnetic field in the collision region was reduced to less than 1 mG by using a double μ -metal shield as well as a Hemholtz coil that eliminated the vertical component of the earth's magnetic field. Typical electron currents were around 10–20 nA, with an energy resolution of 50–70 meV, full width at half maximum. The electron beam could be easily focused at 1 eV and remained stable to within 20% over a period of several days, requiring minor tuning of the spectrometer to maintain the long-term stability of the current to within 5%. The energy of the beam was established by determining the dip in the elastic scattering of the 2^2S He⁻ resonance at 19.366 eV [29] to an uncertainty (over the time of the experiment) of ± 20 meV during a run at a given impact energy E_0 . Typically the contact potential varied by around 0.8–0.9 eV in the course of the experiments. Energy-loss spectra of the elastic peak were collected at fixed E_0 values and electron-scattering angles θ by repetitive multichannel-scaling techniques. The effusive target gas beam was formed by flowing gas through a thin aperture source 0.3 mm in diameter described previously [30], which was sooted to reduce secondary electrons and placed 6 mm below the axis of the electron beam. This tube was incorporated into a movable source arrangement

[31]. The movable gas source method has been well tested previously in our laboratory and determines background scattering rates expediently and accurately in electron-scattering experiments. The vapor pressure behind the source was about 1.5 torr and the pressure in the experimental chamber was 4×10^{-6} torr. In the course of the experiment, it was noted that the background pressure in the chamber rose from $\approx 8 \times 10^{-8}$ to $\approx 4 \times 10^{-7}$ torr when the target source was shut off. This was established to be due to water condensing on the walls of the chamber and on our diffusion pump's double Freon-cooled vapor trap, which operated at a temperature of about 120 K. Eventually, after running for about 1 week to 10 days, we had to isolate the chamber from the diffusion pump system and let the cold trap warm up to release the condensed water. The base pressure of the experimental chamber on reverting to pump down fell back to its normal value of $\approx 8 \times 10^{-8}$ torr.

Toward the end of the experiment, we changed the electron-analyzer entrance apertures from being housed in the entrance nose of the analyzer to being located downstream on a lens before the entrance hemisphere, where previously a pupil had been placed to restrict the depth of field of the analyzer. The pupil (2.5 mm diameter) was instead placed at the nose cone. The reason for this change was to increase the transmission of the analyzer for slow electrons, especially those with residual energies (E_R) below 1 eV. In addition to the present results, we had earlier accumulated data [30] for excitation of the (010) vibrational mode, taken while measuring elastic-scattering DCSs. These earlier DCSs, which were measured at significantly lower target densities than the present work, are also compared to our present measurements. For details of the earlier (and essentially the present) setup, the reader is referred to Ref. [30].

B. Computations

Our calculations invoked the adiabatic approximation [20] to separate the nuclear and vibrational degrees of freedom. In this approximation, the purely electronic scattering problem is solved in the fixed-nuclei approximation at various values of the vibrational coordinates $Q_{1,2,3}$. The fixed-nuclei transition amplitude $f(\vec{k} \rightarrow \vec{k}')$ for scattering from initial electron wave vector \vec{k} to final wave vector \vec{k}' thus becomes $f(\vec{k} \rightarrow \vec{k}'; Q_1, Q_2, Q_3)$, with a parametric dependence on the nuclear coordinates $Q_{1,2,3}$. Matrix elements of this amplitude between vibrational states determine the vibrational transition amplitudes.

The electronic problem was solved using the SMC method [26,27] in the static-exchange plus polarization approximation, with the same one-electron basis set, closed-channel description of polarization effects, and Born-dipole-correction procedure as in earlier work on the electronically elastic cross section [30]. The nuclear problem was treated in perhaps the simplest possible approximation. We factored the vibrational wave function into a product of three functions, one for each normal coordinate, and assumed simple harmonic motion at the experimental frequencies about the equilibrium geometry of Császár *et al.* [32] in each of the normal modes. To evaluate vibrational transition matrix ele-

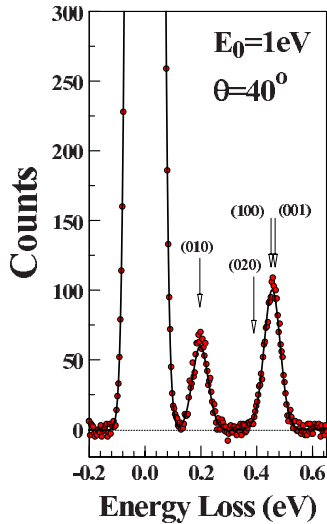


FIG. 1. (Color online) Background-subtracted electron-energy-loss spectrum of H_2O with a typical experimental energy resolution of 60 meV, showing the energy-loss positions of the vibrational modes. The red dots are the experimental data, and the solid line is a fit to those data.

ments, we employed the natural quadrature scheme for harmonic-oscillator functions, Gauss-Hermite quadrature, and because we are interested only in the $v=0$ and $v=1$ levels, we used only a two-point quadrature. The matrix element then reduces to half the difference between $f(+2^{-1/2})$ and $f(-2^{-1/2})$, where $\pm 2^{-1/2}$ is the quadrature abscissa in the dimensionless normal coordinate. We evaluated the Born-correction terms, which are linear in the dipole moment \vec{D} , directly from the difference $\Delta\vec{D} = \vec{D}(+2^{-1/2}) - \vec{D}(-2^{-1/2})$, using the dipole-moment surface of Lodi *et al.* [33] to compute the necessary dipoles.

From a numerical point of view, it should be noted that our $v=0 \rightarrow 1$ vibrational-excitation amplitude is thus the small difference between two large numbers, each of which is subject to uncertainties arising from approximations made and instabilities in the underlying fixed-nuclei, electronically elastic scattering calculations. We may also remark that our procedure, though framed as quadrature, can be thought of alternatively as determining the vibrational matrix element from a finite-difference approximation to the derivative of the electronic scattering amplitude at the equilibrium geometry. In this sense it is akin to methods that evaluate the vibrational transition amplitude from the (analytic) derivative of the electron-molecule potential [21,23]. It should also be noted that our procedure neglects the vibrational inelasticity (that is, we take $|\vec{k}| = |\vec{k}'|$), which becomes an increasingly poor approximation as the impact energy decreases toward threshold.

III. RESULTS AND DISCUSSION

Electron-energy-loss spectra were taken for the elastic peak and the (010) and (100)+(001) vibrational modes of H_2O . A sample spectrum taken at low resolution and high electron current is shown in Fig. 1. These spectra were un-

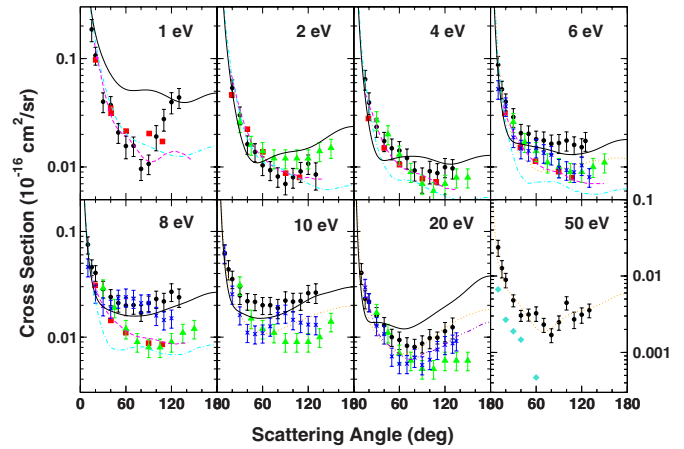


FIG. 2. (Color online) Differential cross sections for electron-impact excitation of the $(000) \rightarrow (010)$ transition (bending mode) in H_2O . Experimental data are from present work (black circles), Seng and Linder [8] (red squares), Shyn *et al.* [11] (green triangles), El-Zein *et al.* [15] (blue \times 's), and Furlan *et al.* [13] (turquoise diamonds at 50 eV). Calculated data are from present work (solid black line), Jain and Thompson [19] (magenta dashed line), Nishimura and Itikawa [21] (orange dotted line), Moreira *et al.* [22] (cyan dot-dashed line), and Čurík and Čárský [23] (violet double-dot-dashed line at 20 eV). Collision energies are as indicated in each panel, except shown for 2 eV panel are data of Refs. [8,22] at 2.1 eV and of Ref. [11] at 2.2 eV; for 4 eV panel, data of Refs. [8,22] at 4.2 eV; and for 8 eV panel, data of Ref. [22] at 7.8 eV and of Ref. [15] at 7.5 eV. Vertical scale at right applies to 50 eV only.

folded to deduce the contributions of the elastic, (010), and (100)+(001) vibrational modes located at 0, 0.198, 0.454, and 0.466 eV, respectively. As in past measurements [8,9,11,14–16], we were unable to observe any significant feature due to the excitation of the (020) mode, i.e., the second harmonic of the bending mode, at an energy loss of 0.396 eV. Energy-loss spectra were taken at incident energies of 1–100 eV for scattering angles of 10° – 130° . The relative spectral intensities were normalized to the elastic DCSs taken recently by us [30]. At scattering angles not covered in Ref. [30], we used spline-interpolated elastic DCSs from Ref. [30]. The relative intensities and vibrational-excitation DCSs are summarized in Table I, while the ICSs and MTCSS obtained from extrapolation of our DCSs to 0° and to 180° are presented in Table II (see Ref. [30] for details of the extrapolation procedure). The quoted uncertainties include those of the elastic DCSs, the uncertainties due to unfolding the spectra, and statistical uncertainties, as well as a conservative estimate of 10% error in the transmission of the spectrometer.

Our results at selected E_0 values are plotted, along with other experimental and calculated results, in Figs. 2 and 3. Our measured DCSs for the excitation of the (010) mode show the forward peak typical of dipole-driven scattering processes. At 1–4 eV, our measured (010) and (100)+(001) DCSs are in excellent quantitative agreement with those measured by Seng and Linder [8], and at 4 eV, agreement is also good with the DCS of Shyn *et al.* [11]. However, at 6 eV, our experimental DCSs are higher at intermediate angles than the previous measurements [8,11,15], which agree well

TABLE I. Inelastic-to-elastic ratios (R) and DCSs for electron-impact excitation of the (010) mode and for the sum of the (100) and (001) modes of water. Uncertainties are 1 standard deviation.

Angle (deg)	R_{010} (%)	Error	$R_{100+001}$ (%)	Error	DCS ₀₁₀ (10^{-18} cm ² sr ⁻¹)	Error	DCS ₁₀₀₊₀₀₁ (10^{-18} cm ² sr ⁻¹)	Error
1 eV								
15	0.678	0.127	0.282	0.046	18.6	4.3	7.73	1.64
20	0.596	0.080	0.350	0.055	10.7	2.0	6.31	1.30
30	0.444	0.070	0.659	0.119	4.00	0.83	5.93	1.33
40	0.652	0.092	1.032	0.159	3.73	0.73	5.91	1.21
50	0.599	0.095	0.924	0.159	2.08	0.43	3.21	0.70
60	0.652	0.124	0.863	0.172	1.56	0.37	2.07	0.50
70	0.889	0.136	1.21	0.25	1.57	0.32	2.13	0.53
80	0.681	0.114	1.13	0.20	0.96	0.21	1.58	0.36
90	0.889	0.140	1.39	0.24	1.07	0.22	1.67	0.36
100	1.74	0.38	2.08	0.43	1.91	0.50	2.29	0.56
110	2.63	0.48	2.77	0.54	2.77	0.63	2.92	0.70
120	3.89	0.69	3.28	0.60	3.97	0.88	3.35	0.76
130	4.25	0.69	3.19	0.56	4.38	0.92	3.28	0.73
2 eV								
20	0.480	0.076	0.308	0.050	5.36	1.00	3.44	0.46
30	0.587	0.078	0.572	0.084	3.01	0.56	2.93	0.42
40	0.559	0.067	0.920	0.139	1.62	0.31	2.67	0.41
50	0.776	0.102	1.41	0.21	1.38	0.26	2.50	0.39
60	0.845	0.094	1.96	0.33	1.04	0.20	2.40	0.38
70	1.05	0.17	2.66	0.40	0.935	0.186	2.36	0.39
80	1.21	0.16	3.17	0.44	0.817	0.167	2.14	0.39
90	1.30	0.19	3.24	0.46	0.698	0.145	1.74	0.34
100	1.83	0.25	3.95	0.61	0.804	0.167	1.73	0.35
110	2.38	0.34	4.74	0.76	0.911	0.190	1.81	0.37
120	2.96	0.41	6.71	1.22	1.07	0.22	2.43	0.46
130	2.30	0.35	8.23	1.30	0.85	0.24	3.05	0.58
4 eV								
15	0.548	0.067	0.582	0.090	6.44	1.34	6.85	1.56
20	0.548	0.087	0.682	0.090	3.93	0.91	4.89	1.04
30	0.626	0.067	1.101	0.125	2.34	0.47	4.13	0.84
40	0.780	0.088	1.86	0.25	1.74	0.35	4.15	0.90
50	1.01	0.14	2.54	0.30	1.49	0.33	3.75	0.77
60	1.27	0.16	3.23	0.40	1.42	0.30	3.60	0.75
70	1.37	0.18	3.75	0.48	1.21	0.26	3.32	0.70
80	1.25	0.14	4.23	0.59	0.928	0.187	3.13	0.68
90	1.26	0.25	4.91	0.58	0.777	0.204	3.04	0.62
100	1.83	0.31	5.91	0.78	0.913	0.216	2.94	0.63
110	2.21	0.32	7.38	0.99	0.88	0.19	2.93	0.63
120	2.84	0.32	7.88	1.20	1.00	0.20	2.76	0.63
130	2.78	0.32	8.39	1.21	0.972	0.198	2.94	0.65

TABLE I. (*Continued.*)

Angle (deg)	R_{010}	Error	$R_{100+001}$	Error	DCS_{010}	Error	$DCS_{100+001}$	Error
	(%)		(%)		(10^{-18} cm ² sr ⁻¹)		(10^{-18} cm ² sr ⁻¹)	
5 eV								
10	0.449	0.086	0.380	0.056	8.68	2.47	7.34	1.88
20	0.473	0.061	0.919	0.118	3.26	0.80	6.34	1.56
30	0.809	0.101	1.218	0.138	2.94	0.72	4.43	1.06
40	0.861	0.095	1.60	0.16	1.91	0.45	3.53	0.82
50	0.795	0.103	2.96	0.35	1.21	0.30	4.52	1.09
60	1.19	0.15	3.76	0.44	1.45	0.36	4.56	1.09
70	1.37	0.16	3.68	0.39	1.38	0.33	3.69	0.87
80	1.16	0.14	4.32	0.48	1.01	0.24	3.76	0.89
90	1.34	0.16	5.93	0.63	1.00	0.24	4.42	1.04
100	1.21	0.14	6.98	0.71	0.741	0.176	4.29	1.00
110	1.75	0.19	8.77	0.88	0.86	0.20	4.33	1.01
120	2.50	0.59	11.5	1.4	1.13	0.36	5.20	1.25
130	3.24	0.57	10.7	1.2	1.48	0.40	4.88	1.16
6 eV								
10	0.530	0.081	0.404	0.064	8.76	1.72	6.67	1.35
15	0.535	0.076	0.704	0.096	5.20	0.98	6.84	1.26
20	0.604	0.077	1.05	0.14	4.01	0.71	6.98	1.28
30	0.819	0.124	1.89	0.25	2.89	0.57	6.68	1.21
40	0.933	0.150	2.71	0.35	2.05	0.42	5.97	1.07
50	1.28	0.17	3.69	0.45	2.03	0.37	5.82	1.01
60	1.38	0.20	4.22	0.56	1.80	0.34	5.53	1.01
70	1.56	0.24	5.03	0.78	1.76	0.35	5.66	1.12
80	1.64	0.26	5.62	0.89	1.64	0.33	5.61	1.13
90	1.91	0.30	6.45	0.90	1.66	0.33	5.63	1.05
100	2.40	0.38	8.58	1.25	1.75	0.35	6.27	1.20
110	2.71	0.38	10.5	1.4	1.60	0.30	6.19	1.15
120	2.74	0.41	10.7	1.7	1.52	0.30	5.96	1.18
125	3.08	0.47	10.4	1.4	1.74	0.34	5.86	1.08
8 eV								
10	0.463	0.066	0.460	0.061	7.50	1.39	7.45	0.99
15	0.460	0.060	0.700	0.080	4.59	0.79	6.99	0.92
20	0.581	0.075	1.03	0.11	4.05	0.68	7.20	0.95
30	0.741	0.092	1.71	0.23	2.84	0.53	6.56	0.86
40	0.961	0.134	2.51	0.30	2.40	0.42	6.25	0.83
50	1.21	0.18	3.27	0.42	2.10	0.38	5.68	0.76
60	1.39	0.19	4.04	0.61	1.99	0.39	5.76	0.76
70	1.63	0.24	5.03	0.63	2.01	0.36	6.17	0.82
80	1.54	0.22	5.76	0.65	1.70	0.29	6.36	0.85
90	2.13	0.26	7.00	0.77	2.09	0.35	6.86	0.90
100	2.78	0.41	8.98	1.21	2.30	0.43	7.41	0.99

TABLE I. (*Continued.*)

Angle (deg)	R_{010}	Error	$R_{100+001}$	Error	DCS_{010}	Error	$DCS_{100+001}$	Error
	(%)		(%)		(10^{-18} cm ² sr ⁻¹)		(10^{-18} cm ² sr ⁻¹)	
110	3.25	0.44	9.81	1.43	2.18	0.42	6.57	0.87
120	3.91	0.54	10.1	1.43	2.68	0.51	6.92	0.92
130	3.23	0.42	7.97	1.21	2.38	0.47	5.87	0.78
10 eV								
10	0.429	0.068	0.383	0.057	6.20	1.27	5.53	1.08
15	0.461	0.075	0.535	0.083	4.38	0.91	5.09	1.02
20	0.510	0.007	0.76	0.10	3.54	0.67	5.28	0.98
30	0.629	0.079	1.14	0.13	2.48	0.45	4.50	0.78
40	0.850	0.107	1.72	0.22	2.19	0.39	4.44	0.80
50	1.15	0.14	2.33	0.26	2.15	0.38	4.36	0.74
60	1.37	0.18	3.00	0.35	2.00	0.37	4.37	0.76
70	1.68	0.22	3.77	0.35	2.00	0.37	4.49	0.71
80	1.77	0.29	4.86	0.60	1.88	0.39	5.18	0.92
90	2.36	0.40	5.80	0.61	2.21	0.47	5.45	0.90
100	2.68	0.41	7.25	0.83	2.16	0.43	5.85	1.00
110	3.27	0.43	8.17	0.95	2.20	0.40	5.50	0.95
120	3.50	0.46	7.81	0.93	2.61	0.48	5.81	1.02
130	3.21	0.54	6.41	0.87	2.64	0.56	5.27	0.98
15 eV								
10	0.364	0.069	0.209	0.036	4.01	0.91	2.30	0.49
15	0.342	0.053	0.231	0.033	2.61	0.52	1.77	0.34
20	0.365	0.057	0.26	0.04	2.15	0.43	1.54	0.30
30	0.443	0.079	0.37	0.06	1.64	0.36	1.38	0.28
40	0.653	0.091	0.56	0.08	1.52	0.29	1.30	0.24
50	0.912	0.123	0.80	0.10	1.39	0.26	1.21	0.22
60	1.29	0.18	1.17	0.15	1.39	0.26	1.26	0.22
70	1.54	0.19	1.64	0.20	1.26	0.22	1.34	0.24
80	1.83	0.24	2.28	0.27	1.29	0.23	1.61	0.28
90	2.19	0.29	3.05	0.40	1.36	0.25	1.89	0.24
100	2.46	0.32	3.75	0.47	1.34	0.24	2.03	0.36
110	3.27	0.48	4.32	0.59	1.61	0.31	2.12	0.40
120	3.00	0.48	3.90	0.59	1.78	0.36	2.32	0.46
130	2.72	0.48	2.82	0.43	2.01	0.43	2.09	0.42
20 eV								
10	0.279	0.051	0.154	0.026	4.06	0.90	2.24	0.48
15	0.234	0.034	0.137	0.019	2.30	0.45	1.35	0.26
20	0.312	0.045	0.155	0.022	2.16	0.42	1.08	0.20
30	0.404	0.056	0.203	0.027	1.60	0.30	0.803	0.149
40	0.612	0.081	0.260	0.032	1.29	0.24	0.549	0.098
50	0.801	0.106	0.344	0.042	1.00	0.19	0.430	0.076
60	1.14	0.16	0.509	0.065	0.939	0.178	0.418	0.076

TABLE I. (Continued.)

Angle (deg)	R_{010}	Error	$R_{100+001}$	Error	DCS_{010}	Error	$DCS_{100+001}$	Error
	(%)		(%)		(10^{-18} cm ² sr ⁻¹)		(10^{-18} cm ² sr ⁻¹)	
70	1.45	0.21	0.765	0.093	0.828	0.159	0.438	0.078
80	1.79	0.23	1.14	0.14	0.806	0.148	0.514	0.092
90	2.27	0.30	1.56	0.20	0.868	0.161	0.596	0.109
100	2.92	0.47	1.88	0.29	0.977	0.202	0.629	0.127
110	2.98	0.50	1.84	0.30	0.989	0.129	0.611	0.079
120	2.84	0.47	1.61	0.24	1.14	0.24	0.644	0.128
130	2.26	0.41	1.25	0.20	1.24	0.28	0.685	0.142
30 eV								
10	0.213	0.035	0.131	0.021	3.30	0.68	2.03	0.41
15	0.205	0.027	0.101	0.013	2.05	0.37	1.01	0.18
20	0.252	0.034	0.095	0.012	1.71	0.31	0.643	0.114
30	0.322	0.041	0.104	0.013	1.06	0.19	0.341	0.059
40	0.491	0.059	0.137	0.016	0.832	0.144	0.232	0.039
50	0.674	0.082	0.166	0.018	0.631	0.110	0.155	0.026
60	0.849	0.108	0.173	0.020	0.498	0.088	0.102	0.017
70	1.10	0.13	0.217	0.019	0.428	0.072	0.085	0.013
80	1.44	0.17	0.345	0.039	0.427	0.073	0.102	0.017
90	1.91	0.23	0.572	0.068	0.476	0.083	0.142	0.024
100	2.71	0.40	0.859	0.122	0.592	0.114	0.188	0.035
110	2.82	0.41	0.587	0.080	0.640	0.123	0.133	0.017
120	2.83	0.43	0.454	0.063	0.930	0.182	0.149	0.028
130	1.97	0.33	0.302	0.045	0.848	0.177	0.130	0.025
50 eV								
10	0.182	0.037	0.0917	0.0138	2.37	0.57	1.20	0.24
15	0.162	0.036	0.0866	0.0142	1.27	0.32	0.68	0.14
20	0.177	0.031	0.0944	0.0125	0.892	0.192	0.477	0.087
30	0.245	0.031	0.173	0.020	0.481	0.086	0.341	0.058
40	0.336	0.035	0.250	0.030	0.305	0.050	0.227	0.040
50	0.676	0.085	0.287	0.037	0.313	0.056	0.133	0.024
60	1.102	0.194	0.377	0.053	0.325	0.070	0.111	0.021
70	1.17	0.19	0.437	0.057	0.231	0.048	0.0862	0.0156
80	1.27	0.21	0.464	0.069	0.169	0.035	0.0616	0.0120
90	2.46	0.42	0.858	0.116	0.248	0.053	0.0866	0.0160
100	4.95	0.75	0.668	0.115	0.447	0.088	0.0603	0.0129
110	2.42	0.51	0.623	0.078	0.271	0.066	0.0699	0.0125
120	1.56	0.29	0.240	0.037	0.312	0.071	0.0480	0.0095
130	1.24	0.20	0.177	0.034	0.357	0.073	0.0510	0.0166
100 eV								
10	0.0970	0.0068	0.0347	0.0041	0.937	0.143	0.335	0.060
15	0.129	0.008	0.0529	0.0050	0.643	0.095	0.264	0.044
20	0.142	0.015	0.0436	0.0082	0.409	0.070	0.125	0.029

TABLE I. (Continued.)

Angle (deg)	R_{010}	Error	$R_{100+001}$	Error	DCS_{010}	Error	$DCS_{100+001}$	Error
	(%)		(%)		(10^{-18} cm ² sr ⁻¹)		(10^{-18} cm ² sr ⁻¹)	
30	0.241	0.025	0.160	0.021	0.197	0.034	0.131	0.024
40	0.362	0.057	0.132	0.034	0.128	0.027	0.0465	0.0137
50	0.366	0.080	0.134	0.049	0.0697	0.0180	0.0256	0.0099
60	0.544	0.129	0.354	0.104	0.0637	0.0173	0.0414	0.0133
70	0.691	0.195	0.364	0.141	0.0522	0.0163	0.0275	0.0113

with each other. On the other hand, our inelastic-to-elastic ratios are quite close to the earlier values. Thus the difference in the vibrational DCSs is due to our larger measured values for the elastic cross section. As discussed previously [30], our implementation of the relative flow method does not depend on an estimate of the effective molecular diameter and may therefore produce more reliable cross sections. At both 6 and 8 eV, our (100)+(001) DCSs are more or less isotropic. At 8 eV, we again see significant differences between our measured DCSs and previous experimental values (including the 7.4 and 7.5 eV DCSs of Makochekanwa *et al.* [17], which are not shown to avoid congestion of the figure but are similar in magnitude to earlier measurements). In the case of the (010) mode, not only the DCSs but the underlying inelastic-to-elastic ratios are different, likely due to the errors arising in resolving the (010) peak from the elastic peak in the energy-loss spectrum. In contrast, our ratios for the stretching modes agree fairly well with previous values. The overall situation at 10 eV is similar to that at 8 eV. At 20 eV, the experimental DCSs are all in fairly good agreement, although our inelastic-to-elastic ratios are closer to those of El-Zein *et al.* [15] than to those of Shyn *et al.* [11]. Finally, at 50 eV, our DCSs are considerably larger than those of

Furlan *et al.* [13]. As seen in Figs. 2 and 3, both the (010) and the (100)+(001) DCSs are forward peaked at 20 and 50 eV (and also at 30 and 100 eV, not shown).

Our calculated (100)+(001) DCSs are considerably larger than previous results away from the forward direction and, from 4 to 10 eV, are in reasonably good agreement with the measured DCSs. However, at 1 and 20 eV, our calculated DCSs are quite different in shape and/or magnitude from the experimental values. As mentioned above, our calculation's neglect of the vibrational inelasticity is a poor approximation near threshold, and this may explain the poor agreement at 1 eV, where the neglected energy loss is nearly half of the impact energy. On the other hand, at energies above the electronic excitation and ionization thresholds, the static-exchange plus polarization approximation used to solve the scattering problem is prone to error because it treats those open channels as closed, and this source of error likely affects our computed result at 20 eV, where previous calculations [21,23] do a much better job. Qualitatively, our (100) and (001) DCSs are similar in magnitude to each other at most angles and energies, though different in their detailed

TABLE II. ICSs and MTCSs for electron-impact excitation of the (100) vibrational mode and for the sum of the (100) and (001) excitations, as a function of impact energy E_0 .

E_0 (eV)	ICS_{010}	Error	$ICS_{100+001}$	Error	$MTCS_{010}$	Error	$MTCS_{100+001}$	Error
	(10^{-17} cm ²)		(10^{-17} cm ²)		(10^{-17} cm ²)		(10^{-17} cm ²)	
1	4.41	1.19	3.89	1.05	4.13	1.12	3.56	0.96
2	1.66	0.37	3.23	0.71	1.24	0.27	3.35	0.74
4	1.70	0.39	4.28	0.99	1.29	0.30	3.94	0.91
5	1.93	0.51	5.67	1.50	1.66	0.44	5.75	1.52
6	2.60	0.59	7.45	1.69	2.38	0.54	7.40	1.68
8	3.13	0.68	7.99	1.74	3.14	0.69	7.94	1.73
10	3.12	0.71	6.43	1.47	3.24	0.74	6.67	1.52
15	2.12	0.51	2.26	0.55	2.25	0.54	2.52	0.61
20	1.44	0.36	0.806	0.200	1.378	0.341	0.812	0.201
30	0.972	0.232	0.245	0.059	0.958	0.229	0.179	0.043
50	0.458	0.113	0.159	0.039	0.404	0.100	0.0907	0.0224
100	0.108	0.028	0.0600	0.0155	0.0632	0.0163	0.0649	0.0121

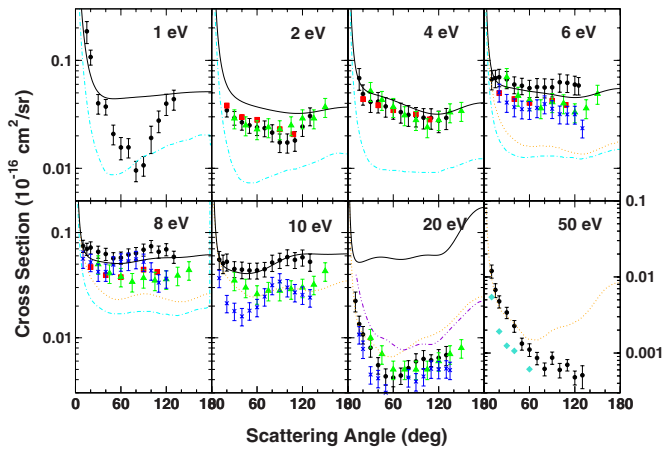


FIG. 3. (Color online) Differential cross sections for electron-impact excitation of the unresolved $(000) \rightarrow (100)$ (symmetric stretch) and $(000) \rightarrow (001)$ (antisymmetric stretch) transitions in H_2O . Experimental data are from present work (black circles), Seng and Linder [8] (red squares), Shyn *et al.* [11] (green triangles), El-Zein *et al.* [15] (blue \times 's), and Furlan *et al.* [13] (turquoise diamonds at 50 eV). Calculated data are from present work (solid black line), Nishimura and Itikawa [21] (orange dotted line), Moreira *et al.* [22] (cyan dot-dashed line), and Āurík and Āárský [23] (violet double-dot-dashed line at 20 eV). Collision energies are as indicated in each panel, except shown for 2 eV panel are data of Refs. [8,22] at 2.1 eV, of Ref. [11] at 2.2 eV, and of Ref. [19] at 2.5 eV; for 4 eV panel, data of Refs. [8,22] at 4.2 eV; and for 8 eV, data of Ref. [22] at 7.8 eV and of Ref. [15] at 7.5 eV. Vertical scale at right applies to 50 eV only.

behavior, as was also found by Nishimura and Itikawa [21]. In contrast, the recent calculations of Moreira *et al.* [22] predict a significantly smaller contribution to the sum from (100) than from (001) , while the experimental data of Allan and Moreira at 1.05 eV [16] and of Makochekanwa *et al.* [17] at 7.5 eV indicate yet another pattern, with the (100) DCS significantly larger than the (001) DCS.

Our calculated results for the (010) mode are also larger than those of previous calculations at intermediate and backward angles, but the differences are not as great as for $(100)+(001)$. As was the case for the bending modes, we find poor agreement between calculation and experiment at 1 and 20 eV, where, as discussed above, the approximations made in the calculation are least accurate. At 2–10 eV, agreement is better. In particular, there is fair agreement with the shape and magnitude of the present experimental DCSs at 6, 8, and 10 eV.

The experimental DCSs were visually extrapolated to zero angle and to 180° and integrated in the usual way to obtain integral and momentum-transfer cross sections. To establish a reasonable estimate of the error due to this process, the integrations were also done with a flat extrapolation of the DCSs at the smallest and largest measured angles. The difference between the integral and momentum-transfer cross sections obtained via the visual and flat extrapolations was taken as the additional error due to the extrapolation and was added in quadrature with the average error of the DCSs to yield an uncertainty for the integral and momentum-transfer cross sections.

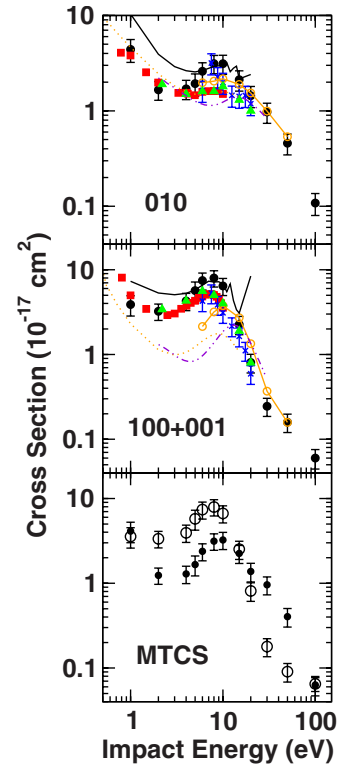


FIG. 4. (Color online) Integral and momentum-transfer cross sections for electron-impact vibrational excitation H_2O . Top panel shows the integral cross sections for the bending mode, middle panel shows the integral cross sections for the unresolved stretching modes, and bottom panel shows the momentum-transfer cross sections. Experimental data are from present work (black circles), Seng and Linder [8] (red squares), Shyn *et al.* [11] (green triangles), and El-Zein *et al.* [15] (blue \times 's). Calculated data are from present work (solid black lines), Nishimura and Itikawa [21] (orange lines with open circles), Nishimura and Gianturco [24] (orange dotted lines), and Āurík and Āárský [23] (violet double-dot-dashed lines). In the bottom panel, filled symbols are the (010) cross sections and open symbols the $(100)+(001)$ cross sections.

The (010) and $(100)+(001)$ integral and momentum-transfer cross sections are shown in Fig. 4. Above 10 eV, the present calculated results show clear indications of pseudo-resonant structure due to the breakdown of the single-open-channel model discussed above. The simple static-exchange approximation should actually work better than static-exchange plus polarization at these energies. Indeed, as seen in Figs. 2–4, the results of Āurík and Āárský [23], which are computed in the static-exchange approximation, are quite close to the experimental data. Below 10 eV, however, our calculated results are smoother and qualitatively reasonable, with maxima and minima at roughly the same energies as seen in the experimental cross sections. Our measured cross sections agree well with those of Seng and Linder [8] at low energies, showing the low-energy rise also seen in the various calculations. Near the broad maximum, our experimental cross sections are somewhat larger than previous measurements, reflecting our larger values for the elastic cross section. At higher energies, they agree well with the calculation of Nishimura and Itikawa [21].

IV. CONCLUSION

We have presented extensive measurements of the cross sections for excitation of the vibrational modes of water by low-energy electron impact. Overall, we observe good agreement with past work for both the inelastic-to-elastic ratios and the vibrational DCSs. However, at intermediate angles and energies from 6 to 20 eV, our larger measured values for the elastic DCSs [30] lead to larger inelastic DCSs. Our calculated cross sections agree reasonably well with the measurements from 2 to 10 eV, but the limitations of the computational model are apparent at higher and lower energies.

ACKNOWLEDGMENTS

This work was sponsored by the U.S. National Science Foundation under Grants No. PHY 0653452 (M.A.K.) and No. PHY 0653396 (V.M. and C.W.). Work by V.M. and C.W. was also supported by the Chemical Sciences, Geosciences and Biosciences Division, Office of Basic Energy Sciences, Office of Science, U.S. Department of Energy, and made use of the Supercomputing and Visualization Facility of the Jet Propulsion Laboratory.

-
- [1] B. Boudaïffa, P. Cloutier, D. Hunting, M. A. Huels, and L. Sanche, *Science* **287**, 1658 (2000).
- [2] B. Boudaïffa, P. Cloutier, D. Hunting, M. A. Huels, and L. Sanche, *Radiat. Res.* **157**, 227 (2002).
- [3] M. A. Huels, B. Boudaïffa, P. Cloutier, D. Hunting, and L. Sanche, *J. Am. Chem. Soc.* **125**, 4467 (2003).
- [4] M. A. Ishii, M. Kimura, and M. Inokuti, *Phys. Rev. A* **42**, 6486 (1990).
- [5] Y. Itikawa and N. Mason, *J. Phys. Chem. Ref. Data* **34**, 1 (2005).
- [6] S. Trajmar, W. Williams, and A. Kuppermann, *J. Chem. Phys.* **58**, 2521 (1973).
- [7] G. Seng and F. Linder, *J. Phys. B* **7**, L509 (1974).
- [8] G. Seng and F. Linder, *J. Phys. B* **9**, 2539 (1976).
- [9] K. Rohr, *J. Phys. B* **10**, L735 (1977).
- [10] K. Jung, Th. Antoni, R. Müller, K.-H. Kochem, and H. Ehrhardt, *J. Phys. B* **15**, 3535 (1982).
- [11] T. W. Shyn, S. Y. Cho, and T. E. Cravens, *Phys. Rev. A* **38**, 678 (1988).
- [12] M. Ben Arfa, F. Edard, and M. Tronc, *Chem. Phys. Lett.* **167**, 602 (1990).
- [13] M. Furlan, M.-J. Hubin-Franskin, J. Delwiche, and J. E. Collin, *J. Chem. Phys.* **95**, 1671 (1991).
- [14] A. El-Zein, M. J. Brunger, and W. R. Newell, *Chem. Phys. Lett.* **319**, 701 (2000).
- [15] A. A. A. El-Zein, M. J. Brunger, and W. R. Newell, *J. Phys. B* **33**, 5033 (2000).
- [16] M. Allan and O. Moreira, *J. Phys. B* **35**, L37 (2002).
- [17] C. Makochekanwa, R. Kajita, H. Kato, M. Kitajima, H. Cho, M. Kimura, and H. Tanaka, *J. Chem. Phys.* **122**, 014314 (2005).
- [18] Y. Itikawa, *J. Phys. Soc. Jpn.* **36**, 1127 (1974).
- [19] A. Jain and D. G. Thompson, *J. Phys. B* **16**, L347 (1983).
- [20] D. M. Chase, *Phys. Rev.* **104**, 838 (1956).
- [21] T. Nishimura and Y. Itikawa, *J. Phys. B* **28**, 1995 (1995).
- [22] O. Moreira, D. G. Thompson, and B. M. McLaughlin, *J. Phys. B* **34**, 3737 (2001).
- [23] R. Čurík and P. Čárský, *J. Phys. B* **36**, 2165 (2003).
- [24] T. Nishimura and F. A. Gianturco, *Europhys. Lett.* **65**, 179 (2004).
- [25] Y. Itikawa, *Int. Rev. Phys. Chem.* **16**, 155 (1997).
- [26] K. Takatsuka and V. McKoy, *Phys. Rev. A* **24**, 2473 (1981).
- [27] K. Takatsuka and V. McKoy, *Phys. Rev. A* **30**, 1734 (1984).
- [28] M. A. Khakoo, C. E. Beckmann, S. Trajmar, and G. Csanak, *J. Phys. B* **27**, 3159 (1994).
- [29] J. H. Brunt, G. C. King, and F. H. Read, *J. Phys. B* **10**, 1289 (1977).
- [30] M. A. Khakoo, H. Silva, J. Muse, M. C. A. Lopes, C. Winstead, and V. McKoy, *Phys. Rev. A* **78**, 052710 (2008).
- [31] M. Hughes, K. E. James, Jr., J. G. Childers, and M. A. Khakoo, *Meas. Sci. Technol.* **14**, 841 (2003).
- [32] A. G. Császár, G. Czakó, T. Furtenbacher, J. Tennyson, V. Szalay, S. V. Shirin, N. F. Zobov, and O. L. Polyansky, *J. Chem. Phys.* **122**, 214305 (2005).
- [33] L. Lodi, R. N. Tolchenov, J. Tennyson, A. E. Lynas-Gray, S. V. Shirin, N. F. Zobov, O. L. Polyansky, A. G. Császár, J. N. P. van Stralen, and L. Visscher, *J. Chem. Phys.* **128**, 044304 (2008).